Sensors **2015**, *15*, 24230-24256; doi:10.3390/s150924230

OPEN ACCESS
sensors
ISSN 1424-8220
www.mdpi.com/journal/sensors

Article

Cell Selection Game for Densely-Deployed Sensor and Mobile Devices In 5G Networks Integrating Heterogeneous Cells and the Internet of Things

Lusheng Wang *, Yamei Wang, Zhizhong Ding and Xiumin Wang

School of Computer and Information, Hefei University of Technology, Anhui 230009, China;
E-Mails: wangyamei_hfut@sina.com (Y.M.); zzding@mail.ustc.edu.cn (Z.D.);
wxiumin@hfut.edu.cn (X.W.)

* Author to whom correspondence should be addressed; E-Mail: wanglusheng@hfut.edu.cn;
Tel.: +86-551-6290-1552.

Academic Editor: Stefan Poslad

Received: 29 July 2015 / Accepted: 12 September 2015 / Published: 18 September 2015

Abstract: With the rapid development of wireless networking technologies, the Internet of Things and heterogeneous cellular networks (HCNs) tend to be integrated to form a promising wireless network paradigm for 5G. Hyper-dense sensor and mobile devices will be deployed under the coverage of heterogeneous cells, so that each of them could freely select any available cell covering it and compete for resource with others selecting the same cell, forming a cell selection (CS) game between these devices. Since different types of cells usually share the same portion of the spectrum, devices selecting overlapped cells can experience severe inter-cell interference (ICI). In this article, we study the CS game among a large amount of densely-deployed sensor and mobile devices for their uplink transmissions in a two-tier HCN. ICI is embedded with the traditional congestion game (TCG), forming a congestion game with ICI (CGI) and a congestion game with capacity (CGC). For the three games above, we theoretically find the circular boundaries between the devices selecting the macrocell and those selecting the picocells, indicated by the pure strategy Nash equilibria (PSNE). Meanwhile, through a number of simulations with different picocell radii and different path loss exponents, the collapse of the PSNE impacted by severe ICI (*i.e.*, a large number of picocell devices change their CS preferences to the macrocell) is profoundly revealed, and the collapse points are identified.

Keywords: Internet of Things; dense sensor networks; heterogeneous cells; cell selection game; inter-cell interference

1. Introduction

After the development of the first four generations, mobile communication systems are encountering new bottlenecks and challenges. On the one hand, many previous hot techniques, such as carrier aggregation, multi-antenna and coordinated multi-point, have been approaching their upper bounds for improving the link-level spectral efficiency [1–3]. On the other hand, existing network facilities for mobile communications are constructed outdoors, but in-building-generated phone calls and data traffic are expected to account for more than half of the total volume in the near future [4,5]. To evolve mobile communication systems toward 5G, a new network paradigm has been raised, called heterogeneous cellular networks (HCNs), which is composed of various types of cells deployed complementarily, forming a heterogeneous environment for wireless devices to access [6–8]. In HCNs, besides macrocells and microcells covering large-scope areas, picocells and femtocells are deployed to cover hotspots and blind zones, so that seamless and ubiquitous access service can be provided at any time anywhere.

In the meantime, the Internet of Things (IoT) is also developing rapidly. Applications, such as smart city [9], Internet of vehicles [10], body area network (BAN) [11] and Internet of bio-nano things [12], were extensively studied, making IoT the most promising concept to integrate the Internet with various domains [13], such as industry, agriculture, healthcare, transportation, markets, education, smart homes, *etc.* Dense deployment will be a new and key feature for future wireless communication systems [14]. Recent studies revealed that IoT and HCNs should integrate to form a new wireless network paradigm for providing real-time and always best connected (ABC) services to both sensor and mobile devices [15,16]. In this network paradigm, mobile devices are able to directly connect to any cell base station (BS) covering it or indirectly connect to a certain BS through a relay. Similarly, sensor devices could also directly transfer data to a BS in the flat networking architecture or indirectly transfer data through a coordinator or relay, such as a mobile device. Figure 1 provides a vision of this network paradigm integrating IoT and HCNs.

Seen from each device's point of view, it is intelligent to always select the best cell for access while under the coverage of multiple overlapped cells. Decisions are made distributedly and rationally by devices themselves (or their coordinators) based on terminal properties (such as velocity and battery state), application types (such as bandwidth demand and latency demand) and user preferences (such as monetary cost and security), forming a cell selection (CS) game among a large amount of densely-deployed sensor and mobile devices. Meanwhile, seen from the system's point of view, all of the devices should be associated with their most appropriate cells, so that the whole system performance can be maximized, called CS optimization.

Studies on the CS game are limited in the literature, as shown by the related work summary in Section 2. However, studies on a similar topic, called network selection (NS), also called access technology selection, are extensive, including NS using game theory [17–21]. Various game models have been used, such as the congestion game, evolutionary game and coalition game. In most of these

studies, the existence of a pure strategy Nash equilibrium (PSNE) has been proven. Compared to NS, CS is much more complicated due to severe inter-cell interference (ICI) [22,23]. Unlike heterogeneous access technologies (such as cellular networks and WiFi) using orthogonal spectra, different types of cells in HCNs usually share the same portion of the spectrum for their transmissions. Taking the scenario where a picocell is deployed in a macrocell as an example, devices around the picocell, no matter which cell they finally select, will have interference from adjacent devices selecting the other cell. Since the deployment of picocells decreases the average inter-BS distance, HCNs bring about much more severe ICI than homogeneous networks.

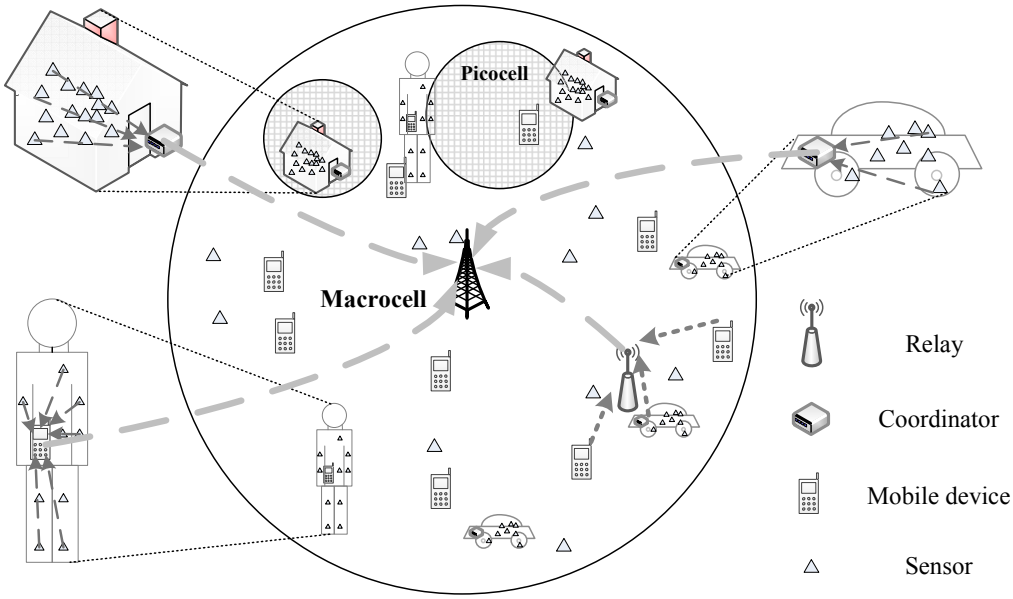

Figure 1. Scenario with multiple picocells and densely-deployed devices in a single macrocell.

To model the CS game with severe ICI, a practical approach is to introduce ICI into the well-known game models for NS. However, this is tough work, because ICI could completely change the features of the payoff functions, hence changing the PSNE in the game. Fortunately, the future network has the key feature of hyper-dense deployment of sensor and mobile devices, guaranteeing the rationality to evaluate the ICI on a given device by taking an average of all of the devices that interfere with it. Meanwhile, no matter whether a device transmits directly or indirectly to a BS, it requires certain resources (*i.e.*, time slot and frequency) and will interfere with near-by devices using the same resource. For the densely-deployed sensors in the near future, coordinators (such as mobiles) will be also densely deployed and be closely surrounded by their sensors. Therefore, the wireless transmission between each coordinator and its BS will also interfere with other transmitters using the same resource.

In this article, we consider a simple, but suitable model, the congestion game [19–21], in which the cost function is defined as the congestion that each device undergoes. Then, we add ICI into the payoff function as a weighted summation of congestion and ICI, changing it into a more complicated game. To further evaluate the features of this game, we also consider channel capacity as the payoff function under the conditions of both fractional frequency reuse (FFR) and orthogonal frequency division (OFD). Three theorems are proven for PSNE in the above games. In the end, extensive simulations show the impact of ICI on the PSNE of these CS games.

The contribution of this study is two-fold. On the one hand, we theoretically find the circular boundary between the devices selecting the macrocell and those selecting picocells, *i.e.*, the PSNE of the CS game among densely-deployed sensor and mobile devices. Three theorems are proven, and their correctness is verified by simulations with the ICI formulated by integrals. On the other hand, we systematically analyze the severe impact of ICI on the PSNE by extensive simulations. The collapse of the PSNE (*i.e.*, a large number of picocell devices changes their CS preferences to the macrocell in the PSNE) and the degradation of the system performance are clearly revealed, which is quite helpful for the future CS scheme design in the HCN and IoT integrated environment.

The remainder of this article is organized as follows. In Section 2, a summary of CS studies is provided. In Section 3, we describe the system model. In Section 4, we theoretically analyze the PSNE of three game models. In Section 5, extensive simulations are performed to demonstrate the correctness of the theorems and the impact of ICI on the CS games and the collapse points. Finally, in Section 6, we draw the conclusions.

2. Related Works

Studies on CS can be traced back to the era of homogeneous networks, such as the work by Hanly [24], Zhang and Letaief [25], Sang *et al.* [26], *etc.* The issue becomes much more complicated when it is in a heterogeneous environment due to the multi-attribute feature of various access technologies and cells. For a heterogeneous wireless network environment composed of WiFi, cellular access technology, personal area networks, *etc.*, NS has been widely studied [17]. Optimization techniques, such as multi-attribute decision making, fuzzy logic and utility theory, have been used for deciding the best network to access. Game theory was also used to study the competition between users for accessing these networks [18].

However, the above two research directions, *i.e.*, CS in homogeneous networks and NS in heterogeneous networks, did not cover the studies on the CS in HCNs, which attracted much attention in recent years. Cells in HCNs not only have a multi-attribute feature, but also suffer from ICI, which brings in new challenges for a CS decision. Existing studies can be divided into two categories, *i.e.*, optimization solutions, as summarized in Table 1, and game theory solutions, as summarized in Table 2. CS optimization was studied from the system-level point of view, *i.e.*, the performance optimization of the whole heterogeneous environment. By contrast, the CS game was studied from the user-level point of view, where each game player rationally aims to improve his/her own benefits. For the two tables, we summarize mainly the mathematical methodologies used in these papers. For simulation studies based on some widely-used parameters, such as reference signal receiving power (RSRP), reference signal receiving quality (RSRQ) and signal-to-interference-plus-noise ratio (SINR), we also point out the key parameters used in their studies. For theoretical studies combining CS with other techniques, such as ICI coordination and resource allocation (RA), we point out that they are joint optimizations or games combining multiple techniques. Considering the scope of this study, we further describe in detail the related studies on CS games in HCNs as follows.

Table 1. Summary of CS optimization of the entire system.

Category	Reference	Features
Range expansion	[27]	SINR
	[28]	Almost blank subframe (ABS), expected user data rate
	[29]	Proportional fairness
	[30]	Bias design
	[31]	Asymmetric downlink/uplink ICI coordination
	[32]	ABS, user association probability, throughput
Association	[33]	Downlink max-min sum rate, convex
	[34]	Total capacity and coverage gains across network
	[35]	Outage probability, average ergodic rate, minimum user throughput
	[36]	Load balancing, gradient descent method, online algorithm
	[37]	Load-aware, best biasing, convex
	[38]	Network capacity, load balancing, pricing based
	[39]	Generalized algebraic framework, load balancing, greedy
	[40]	Energy efficiency, spectral efficiency, cognitive radio
	[41]	Load balancing, distributed near-optimal solution
	[42]	Network utility maximization, proportional fairness, pricing based
Joint CS-RA	[43]	Water filling, bisection search, sum-power and sum-rate constraint
	[44]	Benders' decomposition, non-convex BS association, power control
	[45]	Joint user association, channel assignment, beamforming, power control
	[46]	Orthogonal, co-channel, partially shared, non-convex integer program
	[47]	Maximum capacity, max-min fairness
Fast CS	[48]	Gain in throughput
	[49]	SINR
Performance evaluation	[50]	SINR, capacity
	[51]	SINR, RSRP, RSRQ
	[52]	RSRP, range expansion with static/adaptive offset or with ABS
	[53]	Path loss, SINR, capacity
Others	[54]	Knapsack, assignment problem
	[55]	Maximum expected bitrate
	[56]	Maximum ergodic capacity
	[57]	Percentage of the total earned profit
	[58]	Aggregate energy consumption

Lin *et al.* [59] provided a general form of the CS game and proved the existence of PSNE. Yuan *et al.* [60] studied the case where a femtocell changes from closed access to open access, so that nearby users could access it instead of accessing the macrocell, which decreased uplink ICI from these

users to the femtocell. A Stackelberg game was considered between the femtocell BS as the leader and the macrocell user as the follower to improve their performance by establishing links between them. Moon and Cho [61] proposed a CS algorithm based on competition among a group of users, each of which decided the probability of choosing a microcell as its serving cell. Haddad *et al.* [62] considered a Bayesian game and showed by means of a Stackelberg formulation that the operator could optimize its global utility while the end-users maximized their individual utilities. Liu *et al.* [63] proposed a Nash bargaining solution, which formulated the user association optimization as a Nash bargaining problem, so as to maximize the sum data rate related utility of all users in the overall system while guaranteeing the user's minimal data rate and considering user fairness. Gao *et al.* [64] modeled the game on two levels, *i.e.*, inter-cell CS game and intra-cell RA game, proved that the CS game had mixed strategy Nash equilibrium (MSNE) and proposed a distributed algorithm that converged to MSNE.

Table 2. Summary of the CS game between devices.

Category	Reference	Features
General form	[59]	PSNE existence proof
Evolutionary	[65]	Reinforcement learning to search for evolutionary equilibrium
Stackelberg	[60]	Femtocell changes from closed to open access against uplink ICI
Bargaining	[63]	ICI coordination, Nash bargaining solution
Bayesian	[62]	Maximum throughput, Stackelberg formulation
Joint CS-RA	[64]	MSNE existence prove, distributed algorithm converges to MSNE
Competition	[61]	Probability to select certain cell
Congestion	[66]	Prove of PSNE under inter-cell interference
Learning based	[67]	Minimize the number of outages
	[68]	Distributed decision making toward PSNE
	[69]	Predict best cell during handover decision

Some studies considered intelligent learning algorithms to search for the PSNE. Feng *et al.* [65] proposed an evolutionary game model for CS in a two-tier femto/macro scenario, and the reinforcement learning algorithm was used to search for the evolutionary equilibrium. Tan *et al.* [68] studied the CS problem in a two-tier femtocell network. To achieve PSNE without a centralized controller, the Q-learning algorithm was used to help distributed individual users adapt and make decisions independently. Dhahri and Ohtsuki [69] proposed a Q-learning-based CS scheme, which predicted the best cell by the Q-learning algorithm during the handover procedure, so it improved the system capacity, avoided unnecessary handovers and decreased signaling cost. Kudo and Ohtsuki [67] proposed a scheme to select a cell by the Q-learning algorithm to minimize the number of outages from its past experience independently. Liao *et al.* [66] tried to embed ICI into the CS congestion game in a scenario with one macrocell and one picocell. PSNE was analyzed in both theoretical and simulative ways. In this article, for densely-deployed sensor and mobile devices in HCNs with multiple picocells, we work

on the analysis of PSNE collapse toward the macrocell impacted by severe ICI and the corresponding degradation of system performance, which is not revealed by any of the above studies.

3. System Model

We consider the case where a single macrocell BS_0 and a set of open access picocells $\{BS_i \mid i = 1, ..., M\}$ coexist and overlap with one another. We ignore the macrocells around this single macrocell, because ICI between heterogeneous cells obviously has a higher magnitude than ICI between homogeneous cells, so this simplification does not affect the results much. There are in total N_0 densely-deployed sensor and mobile devices in the scenario, given by $\mathbf{DV}_{All} = \{DV_j | j = 1, ..., N_0\}$. Note that the assumption of the dense deployment of the devices guarantees the rationality to evaluate the ICI on a given device by taking an average of all of the devices that interfere with it, as analyzed in Section 4.2 later. The cell radius of BS_i is denoted by R_i, and the number of devices under the coverage of BS_i is given by N_i. We assume that all of the devices are uniformly distributed within the disc coverage area of BS_0, so the density of devices is given by $\rho = N_0/\pi R_0^2$. $N_i = N_0 R_i^2/R_0^2, \forall i \in \{1, ..., M\}$. Main notations are summarized in Table 3. Without a specific description, notations follow the rule that, the subscript $i = 0$ represents the macrocell and $i \in \{1, ..., M\}$ represents the i-th picocell.

Table 3. Main notations.

BS_i	BS of cell i
$\mathbf{DV}_i$	Devices selecting BS_i
$\mathbf{DV}_{All}$	All of the devices within the coverage of the macrocell disc area
DV_j	The j-th device in a set of devices
N_i	Number of devices within the coverage of cell i
R_i	Radius of the disc area covered by BS_i
P_i	Uplink transmission power of the devices to BS_i
B_i	Total available bandwidth for cell i
I_{ij}	Average ICI from the devices in cell BS_i to BS_j
n_i	Number of devices selecting BS_i
D_{ij}	Distance between BS_i and BS_j
d_{ij}	Distance between BS_i and DV_j
r_i	Radius of the disc area formed by the devices selecting cell i
p_j	Pure strategy of DV_j
U_j / C_j	Utility/cost function of DV_j

Devices selecting $BS_i, i \in \{1, ..., M\}$ are given by $\mathbf{DV}_i$. Data can be transmitted directly between the BS and a device or indirectly through a coordinator (or relay). For indirect transmission through a coordinator, we assume that the link between the BS and the coordinator is wireless, so it is identical to the case when the coordinator itself transmits to the BS. Meanwhile, transmissions between sensors and their coordinators are on unlicensed frequency bands with extremely low transmission power, which do not cause ICI and do not even occupy resources in licensed bands. In a word, direct and indirect connections can be modeled identically for evaluating ICI in the CS game. We assume that all of the

devices are identical for their traffic type, terminal property and user preference, so it is reasonable to assume that $\mathbf{DV}_i$ are the n_i devices closest to BS_i, forming a disc area with radius r_i, and $n_i = N_0 r_i^2 / R_0^2$, as demonstrated by the azure circle in Figure 2. If the above features of various devices are not identical in reality, a function combining these features is used to represent the unified tendency for selecting each cell, which can be considered as a virtual distance when mapping into our system model. Therefore, the above assumption still holds when those features are not identical, while the n_i devices are the closest to BS_i in terms of the virtual distance (corresponding to the n_i devices with the highest tendency to BS_i). The objective of this study is to identify n_i corresponding to the PSNE of the game below:

$$\mathscr{G} = \{\mathbf{DV}_{All}, (p_j)_{j\in\{1,\ldots,N_0\}}, (U_j)_{j\in\{1,\ldots,N_0\}}\} \tag{1}$$

where $\mathbf{DV}_{All}$ are the players, $\mathbf{p} = \{p_j | j = 1, \ldots, N_0\}$ are the pure strategies used by the players, each player's strategy is chosen from the pure strategy set $\{BS_i | i = 0, 1, \ldots, M\}$ and $(U_j)_{j\in\{1,\ldots,N_0\}}$ are the players' payoff functions, which are assumed to be identical and related to the number of devices selecting the same cell, the positions of devices and ICI. Equation (1) is a class of non-cooperative game, called the congestion game, as long as $\forall j \in \{1, \ldots, N_0\}$; U_j is a utility function of the number of devices selecting the same BS with a monotonically non-increasing feature (or non-decreasing feature if congestion C_j is used as a cost function).

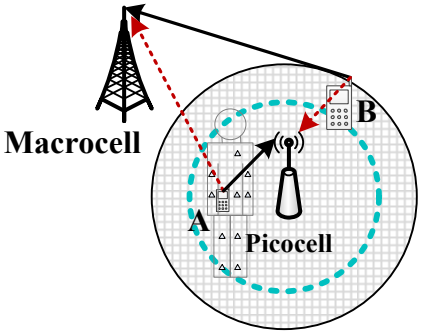

Figure 2. System model. Each picocell holds a circular boundary (*i.e.*, the azure dashed circle) indicating the PSNE. Device A is inside the boundary, so it transmits to the picocell and interferes with the macrocell. Although Device B is within the edge of the picocell, it is outside of the dashed circle, so it selects the macrocell and interferes with the picocell.

Given pure strategies $\mathbf{p}$, PSNE is defined as [70]:

Definition 1. *A set of pure strategies,* $\mathbf{p}^*$ *is called a PSNE if* $\forall j \in \{1, \ldots, N_0\}$ *and* $\forall p_j \in \mathbf{p}$,

$$U_j(p_j^*, p_{-j}^*) \geq U_j(p_j, p_{-j}^*) \tag{2}$$

Based on the assumptions above, given a set $\mathbf{n}^* = \{n_i | i = 1, \ldots, M\}$, $\mathbf{p}^*$ is fixed, so the definition of PSNE could be changed into the following:

Definition 2. $\mathbf{n}^*$ *is said to be a PSNE if its corresponding* $\mathbf{p}^*$ *satisfies Definition 1.*

4. Cell Selection Games

Since picocells usually have a small coverage and are deployed at hotspots for complementation, we assume that their coverage areas are independent of one another. In this scenario, we are interested in n_i^*, the number of devices selecting BS_i in the PSNE.

4.1. Traditional Congestion Game

We use the traditional congestion game (TCG) to model the CS problem with multiple picocells. In this model, congestion of a device is proportional to the total number of devices selecting the same BS, so the cost of DV_k selecting the macrocell BS_0 and the cost of DV_l selecting picocell $BS_i, i \in \{1, ..., M\}$ can be the inverse of the amount of resource obtained by DV_k and DV_l, written as:

$$C_k(BS_i, p_{-k}) = \frac{n_i}{B_i} \tag{3}$$

$$C_l(BS_0, p_{-l}) = \frac{N_0 - \sum_\alpha n_\alpha}{B_0} \tag{4}$$

where B_0 and B_i represent the total uplink bandwidth for BS_0 and BS_i, respectively.

If DV_k changes the CS preference to BS_0, its cost becomes:

$$C_k(BS_0, p_{-k}) = \frac{N_0 - \sum_\alpha n_\alpha + 1}{B_0} \tag{5}$$

Similarly, if DV_l changes the CS preference to BS_i, its cost becomes:

$$C_l(BS_i, p_{-l}) = \frac{n_i + 1}{B_i} \tag{6}$$

Theorem 1. *For TCG,* $\forall i \in \{1, ..., M\}$*, define:*

$$g_1(n_i) = n_i + \frac{B_i}{B_0 + B_i} \sum_{\alpha \neq i} n_\alpha \tag{7}$$

$$A_{1,i} = \frac{B_i(N_0 + 1)}{B_0 + B_i} \tag{8}$$

(1) if $g_1(N_i) < A_{1,i}$*,* $n_i^* = N_i$ *forms the PSNE;*
(2) if $g_1(1) > A_{1,i}$*,* $n_i^* = 0$ *forms the PSNE;*
(3) otherwise, n_i^* *satisfying* $A_{1,i} - 1 \leq g_1(n_i^*) \leq A_{1,i}$ *forms the PSNE.*

Proof. Based on Definition 1, we rewrite the conditions that n_i forms the PSNE as, $\forall i \in \{1, ..., M\}$:

$$C_k(BS_i, p_{-k}) \leq C_k(BS_0, p_{-k}) \tag{9}$$

$$C_l(BS_0, p_{-l}) \leq C_l(BS_i, p_{-l}) \tag{10}$$

Equations (9) and (10) separately indicate that no device selecting the picocell BS_i and the macrocell BS_0 feels like changing the CS preference.

Taking Equations (3)–(6) into (9) and (10), we get:

$$A_{1,i} - 1 \leq g_1(n_i^*) \leq A_{1,i} \tag{11}$$

To prove the existence of a PSNE based on Equation (11), we consider firstly the two-dimensional case with n_1 and n_2 shown in Figure 3. For $A_{1,1} - 1 \leq g_1(n_1) \leq A_{1,1}$, the integer points between the two parallel solid lines fit it. Since the distance between Point A and B is one and the slope coefficient of the two solid lines corresponding to the above inequation is less than -1, given each n_1, there is at least one integer solution for n_2.

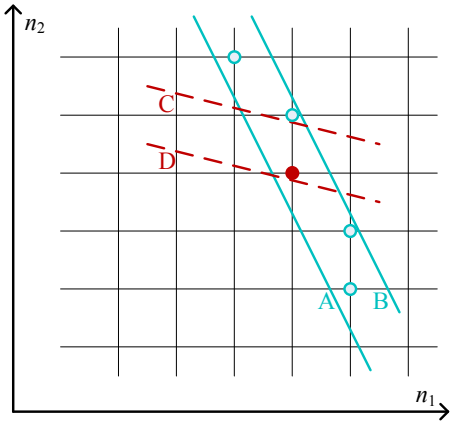

Figure 3. Two-dimensional case of the traditional congestion game (TCG) for the proof of Theorem 1.

Meanwhile, since the slope coefficient of the two parallel dashed lines for $A_{1,2} - 1 \leq g_1(n_2) \leq A_{1,2}$ is in $(-1, 0)$ and the distance between Point C and D is one, at least one integer solution between the two solid lines fits for the above inequation, *i.e.*, at least one solution can be found for Equation (11) with $i = 1, 2$.

Applying mathematical induction, $\forall\{n_1, n_2, ..., n_k\}$ as a k-dimensional point in the k-dimensional case, there is at least one integer solution for n_{k+1}. Since the two parallel dashed lines in the $(k+1)$-th dimension have a slope coefficient in $(-1, 0)$, at least one integer solution fits for $A_{1,k+1} - 1 \leq g_1(n_{k+1}) \leq A_{1,k+1}$, indicating the existence of a PSNE.

Since BS_i covers N_i devices, if $g_1(N_i) < A_{1,i}$, the PSNE corresponds to $n_i^* = N_i$, indicating that all of the devices covered by BS_i select it. If $g_1(1) > A_{1,i}$, the PSNE corresponds to $n_i^* = 0$. Otherwise, n_i^* satisfying Equation (11) forms the PSNE.

To sum up, Theorem 1 indicates the numbers of devices selecting different picocells in the PSNE. $g_1(n_i)$ in Theorem 1 is a combination of the variables representing the numbers of devices selecting different picocells. When this combined value satisfies Theorem 1, a PSNE is reached.

4.2. Congestion Game with ICI

The deployment of heterogeneous cells decreases the inter-BS distance on average, which severely increases ICI. The congestion model in the previous subsection is simple, but it does not take ICI into account. In this subsection, we consider the game with a cost function combining congestion and ICI linearly, called the congestion game with ICI (CGI).

Since the device that interferes with the device DV_j is highly related to the RA strategy and can be any device selecting adjacent cells, the estimation of the ICI for a general CS problem is quite difficult. The study in this article focuses on the scenario with densely-deployed devices, where the average ICI from devices in other cells can be used to represent the ICI that DV_j undergoes. Therefore, a device's uplink transmission to the picocell BS_i undergoes an average ICI from devices using the macrocell BS_0, which is a function of n_i, given by:

$$I_{0i}(n_i) = \frac{GP_0}{N_0 - \sum_\alpha n_\alpha}\left(\sum_{j \in \mathbf{DV}_{All}} \frac{1}{d_{ij}^\gamma} - \sum_\alpha \sum_{j \in \mathbf{DV}_\alpha} \frac{1}{d_{\alpha j}^\gamma}\right) \tag{12}$$

where P_0 is the transmission power of the devices to BS_0, γ is the path loss exponent, $G = G_t G_r \lambda^2 / 4\pi^2$ is a constant related to transmission antenna gain G_t, reception antenna gain G_r and wavelength λ. Note that we do not consider shadowing or multipath fading due to the fact that our model and analysis are statistical for densely-deployed sensor and mobile devices, so the instantaneous signal strength of a particular device does not affect the integral results much.

Compared to R_0, the radius of the picocell R_i is small, so we ignore the position difference of the devices in it when calculating the average interference to BS_0, given by:

$$I_{i0} = \frac{GP_i}{D_{0i}^\gamma} \tag{13}$$

where P_i is the transmission power of the devices to BS_i.

Therefore, the cost of DV_k using BS_i is given by:

$$C_k(BS_i, p_{-k}) = \frac{n_i}{B_i} + wI_{0i}(n_i) \tag{14}$$

where w is the weight of ICI, which is required, because ICI and congestion have different magnitudes and are difficult to normalize. w should not be too large, otherwise it changes the monotonicity of Equation (14), and the PSNE will collapse to the macrocell without any equilibrium between N_i and zero. Figure 4a shows that, once a picocell device decides to select the macrocell, it leads to a much faster increment of the cost for other devices still preferring the picocell. Therefore, devices will change their preferences one by one until an equilibrium is reached where only a few devices or even no device still prefers the picocell.

Similarly, the cost of DV_l using BS_0 is given by:

$$C_l(BS_0, p_{-l}) = \frac{N_0 - \sum_\alpha n_\alpha}{B_0} + wI_{i0} \tag{15}$$

After DV_k changes the CS preference to BS_0, its cost becomes:

$$C_k(BS_0, p_{-k}) = \frac{N_0 - \sum_\alpha n_\alpha + 1}{B_0} + wI_{i0} \tag{16}$$

Since ICI is related to the positions of devices, we assume that the device that has the strongest willingness to change the CS preference to BS_i is the one closest to the circular boundary. Therefore, after DV_l changes the CS preference to BS_i, its cost becomes:

$$C_l(BS_i, p_{-l}) = \frac{n_i + 1}{B_i} + wI_{0i}(n_i + 1) \tag{17}$$

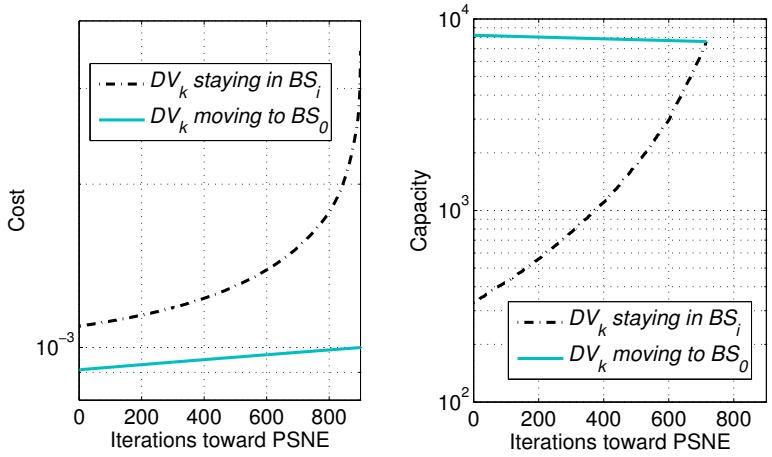

(a) **(b)**

Figure 4. Monotonicity of payoff functions in Theorems 2 and 3. Obtained by setting $B_i = 2/3B_0$, $R_i = 300$ m, $w = 3 \times 10^6$ and other parameters commonly configured as in Section 5, for a scenario with one picocell located within the macrocell. Curves are obtained by searching for the PSNE, so the number of devices selecting the picocell gradually decreases during iterations. (**a**) Cost in Theorem 2; (**b**) capacity in Theorem 3.

Theorem 2. *For CGI, define:*

$$g_2(n_i) = n_i + \frac{B_i}{B_i + B_0} \sum_{\alpha \neq i} n_\alpha + \frac{B_i B_0}{B_i + B_0} w I_{0i}(n_i) \tag{18}$$

$$A_{2,i} = \frac{B_i}{B_i + B_0}(N_0 + 1 + B_0 w I_{i0}) \tag{19}$$

(1) if $g_2(N_i) < A_{2,i}$, $n_i^* = N_i$ *forms the PSNE;*
(2) if $g_2(1) > A_{2,i}$, $n_i^* = 0$ *forms the PSNE;*
(3) otherwise, n_i^* *satisfying* $g_2(n_i^*) \leq A_{2,i} \leq g_2(n_i^* + 1)$ *forms the PSNE.*

Proof. Based on Definition 1, we obtain the conditions for the PSNE of CGI as follows:

$$C_k(BS_i, p_{-k}^*) \leq C_k(BS_0, p_{-k}^*) \tag{20}$$

$$C_l(BS_0, p_{-l}^*) \leq C_l(BS_i, p_{-l}^*) \tag{21}$$

Equations (20) and (21) indicate separately that no device selecting BS_i and BS_0 feels like changing the CS preference.

Taking Equations (14)–(17) into (20) and (21), we get:

$$g_2(n_i^*) \leq A_{2,i} \leq g_2(n_i^* + 1) \tag{22}$$

To sum up,

(1) If $g_2(N_i) < A_{2,i}$, all of the devices under the coverage of BS_i select it, and $n_i^* = N_i$ forms the PSNE.
(2) If $g_2(1) > A_{2,i}$, all of the devices under the coverage of BS_i select BS_0, and $n_i^* = 0$ forms the PSNE. This case cannot be indicated by Equation (22) because the integral for $I_{0i}(n_i)$ is equivalent to an

extremely large number of devices deployed in the area. In such a case, there is absolutely one device collocated with BS_i, leading to infinity for $g_2(0)$.

(3) Otherwise, n_i^* satisfying Equation (22) forms the PSNE. Since $I_{0i}(n_i)$ is a decreasing function with quite a small value, as long as w is kept below a certain threshold, the gap between $g_2(n_i^*)$ and $g_2(n_i^*+1)$ is smaller than one, so there is always at least one n_i^* satisfying it.

4.3. Congestion Game with Capacity

The game model in the previous subsection focuses on the linear combination of congestion and ICI, so the precision of such a game depends on the weight of ICI. We look for a more realistic payoff function to represent the impact of ICI, so channel capacity is considered in this subsection. We first consider the case where FFR for ICI coordination is adopted by picocells, called the congestion game with capacity under the condition of FFR (CGC-FFR), so the utility functions can be written as follows.

The channel capacity of DV_k selecting the picocell BS_i is:

$$U_k(BS_i, p_{-k}) = \frac{B_i}{n_i}\log_2\left(1+\frac{GP_i/d_{ik}^{\gamma}}{\sigma^2+I_{0i}(n_i)}\right) \tag{23}$$

where σ^2 represents the variance of additive white Gaussian noise (AWGN). Due to the fact that the device on the edge of the circular boundary has the strongest willingness to change the CS preference, d_{ik} is used as the distance between DV_k and BS_i. If DV_k changes preference to the macrocell BS_0, its channel capacity becomes:

$$U_k(BS_0, p_{-k}) = \frac{B_0}{N_0-\sum_{\alpha} n_{\alpha}+1}\log_2\left(1+\frac{GP_0/D_{0i}^{\gamma}}{\sigma^2+I_{i0}}\right) \tag{24}$$

Figure 4b shows the monotonicity of the above two payoff functions. The curves show that, when the devices gradually change their preferences to the macrocell, the other devices' willingness (*i.e.*, the capacity) to select the picocell increases, while their willingness to select the macrocell decreases. When the two curves meet after 716 iterations, an equilibrium is reached.

Similarly, the channel capacity of DV_l selecting BS_0 is:

$$U_l(BS_0, p_{-l}) = \frac{B_0}{N_0-\sum_{\alpha} n_{\alpha}}\log_2\left(1+\frac{GP_0/D_{0i}^{\gamma}}{\sigma^2+I_{i0}}\right) \tag{25}$$

If DV_l hands over to BS_i, its channel capacity is:

$$U_l(BS_i, p_{-l}) = \frac{B_i}{n_i+1}\log_2\left(1+\frac{GP_i/d_{il}^{\gamma}}{\sigma^2+I_{0i}(n_i+1)}\right). \tag{26}$$

Theorem 3. *For CGC-FFR, define:*

$$g_3(n_i) = \log_2\left(1+\frac{GP_i[N_0/(n_iR_0^2)]^{\gamma/2}}{\sigma^2+I_{0i}(n_i)}\right)^{\frac{N_0-\sum_{\alpha} n_{\alpha}+1}{n_i}} \tag{27}$$

$$A_{3,i} = \log_2\left(1+\frac{GP_0/D_{0i}^{\gamma}}{\sigma^2+I_{i0}}\right)^{\frac{B_0}{B_i}} \tag{28}$$

(1) if $g_3(N_i) > A_{3,i}$, $n_i^* = N_i$ forms the PSNE;

(2) if $g_3(1) < A_{3,i}$, $n_i^* = 0$ *forms the PSNE;*
(3) otherwise, n_i^* *satisfying* $g_3(n_i^* + 1) \leq A_{3,i} \leq g_3(n_i^*)$ *forms the PSNE.*

Proof. Based on Definition 1, we obtain the conditions for the PSNE of CGC-FFR as follows:

$$U_k(BS_i, p_{-k}^*) \geq U_k(BS_0, p_{-k}^*) \tag{29}$$

$$U_l(BS_0, p_{-l}^*) \geq U_l(BS_i, p_{-l}^*) \tag{30}$$

Since all of the devices are assumed identical, the device most preferably changing its preference is the one on the edge of the blue circle in Figure 2, so:

$$d_{ik}^{\gamma} = \left(\frac{R_0^2 n_i^*}{N_0}\right)^{\gamma/2} \tag{31}$$

$$d_{il}^{\gamma} = \left[\frac{R_0^2 (n_i^* + 1)}{N_0}\right]^{\gamma/2} \tag{32}$$

Taking Equations (23)–(26), (31) and (32) into Equations (29) and (30), we get:

$$g_3(n_i^* + 1) \leq A_{3,i} \leq g_3(n_i^*) \tag{33}$$

To sum up,

(1) If $g_3(N_1) \geq A_{3,i}$, all of the devices under the coverage of BS_i select it, so $n_i^* = N_i$ forms the PSNE.
(2) If $g_3(1) < A_{3,i}$, similar to the explanation in the proof of Theorem 2, $n_i^* = 0$ forms the PSNE.
(3) Otherwise, $\mathbf{n}^*$ satisfying Equation (33) forms the PSNE.

To evaluate the impact of ICI in CGC-FFR, we also consider a basic case where OFD between picocells and the macrocell is adopted, *i.e.*, picocells use B_i and the macrocell uses $B_0 - B_i$, called the congestion game with capacity under the condition of OFD (CGC-OFD). In this case, ICI is completely eliminated, so $g_3(n_i)$ and $A_{3,i}$ in Theorem 3 are changed into:

$$g_4(n_i) = \log_2\left(1 + \frac{GP_i[N_0/(n_i R_0^2)]^{\gamma/2}}{\sigma^2}\right)^{\frac{N_0 - \sum_{\alpha} n_{\alpha} + 1}{n_i}} \tag{34}$$

$$A_{4,i} = \log_2(1 + \frac{GP_0/D_{0i}^{\gamma}}{\sigma^2})^{\frac{B_0 - B_i}{B_i}} \tag{35}$$

5. Performance Evaluation

In this section, we provide extensive simulations by MATLAB to demonstrate the correctness of the theorems and the impact of ICI on the PSNE for the CS games with a large amount of densely-deployed devices in HCNs. The simulation area is a single macrocell with a radius equaling 1000 m. A small number of picocells are almost randomly deployed within the coverage of the macrocell, but assuming that they do not overlap with one another. This is achieved by randomly choosing the picocells' locations one-by-one and making sure each one is not overlapped with those already deployed.

Since this study considers the uplink, the transmission power is set to 23 dBm for devices selecting the macrocell [71]. By contrast, the transmission power for the devices selecting picocells should be less

than this because of power control, expanding from −9–10 dBm, adjusted to fit for different picocell sizes and path loss exponents. Each macrocell uses the total uplink bandwidth of the system, *i.e.*, 10 MHz, while picocells get part of the total uplink bandwidth because of the ICI coordination for picocells in HCNs. The AWGN spectral density is set to −174 dBm/Hz, and the radio frequency is set to 1.9 MHz. We set the density to 10^5 devices/macrocell with a uniform distribution within its cell coverage. The maximum number of rounds of simulations for obtaining each point in the following figures is 100, and each round has newly deployed positions of the picocells, as well as the devices.

In each round, we use the method proposed by I. Milchtaich in [72] to search for the PSNE. The method is to check each player's willingness to change strategy, and the searching process reaches a PSNE if no player feels like making further changes. This method guarantees the convergence to the PSNE in just a few iterations for congestion games, so it fits quite well for this study.

5.1. Verification of the Theorems

In this subsection, the three theorems are verified by simulations. Three picocells with radii of 100, 200 and 300 m are randomly deployed, and their PSNE are obtained by the Milchtaich method. Then, we take the PSNE into the theorems to verify their correctness.

For Theorem 1, by increasing B_i, we can see that both $g_1(n_i)$ and $A_{1,i}$ increase, and $g_1(n_i)$ is perfectly located between $A_{1,i} - 1$ and $A_{1,i}$. When B_i is larger than a certain threshold for each cell radius, all of the devices under the coverage of this picocell select it, so the curve of $g_1(n_i)$ leaves $A_{1,i} - 1$ by keeping $n_i^* = N_i$ for the PSNE, as shown in Figure 5a.

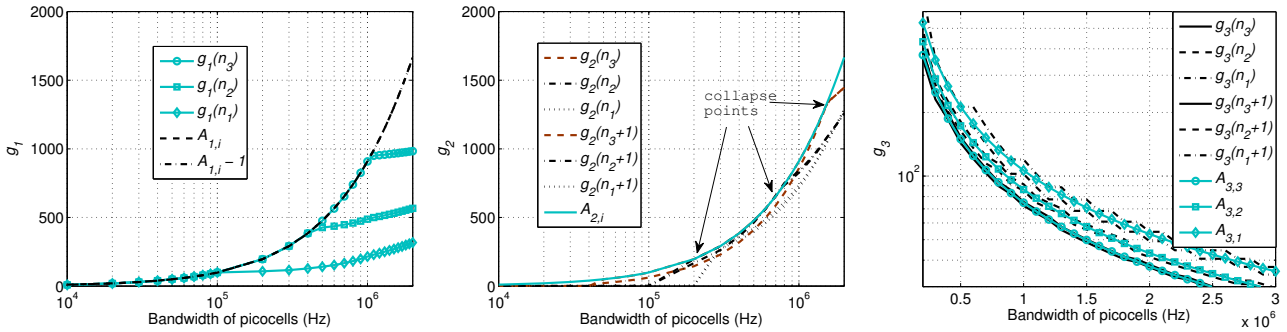

(a) **(b)** **(c)**

Figure 5. Verification of the theorems. (**a**) Theorem 1; (**b**) Theorem 2; (**c**) Theorem 3.

For Theorem 2, we set the transmission power of the devices selecting the three picocells as −9, −3 and 0.5 dBm, so that their coverage increases proportionally. The calculation of $g_2(n_i)$ is not based on the ICI obtained by Equation (12), which is unstable due to the instantaneous distribution of the devices. Instead, Equation (A15) obtained in the Appendix, as an average value, is used. Note that this average value is derived under the condition $\gamma = 2$, so that a closed-form expression as an analytical result can be obtained to compare to the simulation results and to validate the theorems. Based on our experience, when w is relatively small, the result of CGI is quite similar to that of TCG. By contrast, when w is larger than a threshold, the PSNE collapses to all zeros, *i.e.*, all of the devices select the macrocell. Therefore,

we choose $w = 10^6$ to show this phenomenon in Figure 5b. We can see that $A_{2,i}$ is not within $g_2(n_i)$ and $g_2(n_i + 1)$, except for the three collapse points, one for each picocell. In detail, before each collapse point (*i.e.*, on the right side), the PSNE have $n_i^* = N_i$. While after each collapse point (*i.e.*, on the left side), the PSNE collapse to all zeros, so the curves leave $A_{2,i}$ immediately.

For Theorem 3, the same configuration as above is used. To show clearly the relationship between $g_3(n_i)$ and $A_{3,i}$, the total bandwidth of picocells (*i.e.*, the x-axis) is set to [0.2, 3] MHz. We can see that the curves for $A_{3,i}$ are smooth, while the curves for $g_3(n_i)$ and $g_3(n_i + 1)$, as functions of n_i, are slightly fluctuating. $\forall i \in \{1, 2, 3\}$, $A_{3,i}$ is perfectly located between $g_3(n_i)$ and $g_3(n_i + 1)$, indicating the correctness of Theorem 3.

5.2. Impact of ICI by Comparing TCG and CGI

In this subsection, we randomly deploy five picocells with identical radii in each round of simulation. For different curves in each figure, the radii of picocells vary from 100–300 m. In order to achieve different coverage radii for picocells, we set the transmission power for devices selecting picocells as -9, -3 and 0.5 dBm for picocell radii equaling 100, 200 and 300 m when the path loss exponent is two (free space). When the path loss exponent is three (suburbs), the transmission power is set to -9, 0 and 5.3 dBm, respectively. Additionally, when the path loss exponent is four (downtown), they are set to -9, 3 and 10 dBm. Because the magnitude of ICI changes along with the change of the path loss exponent, the collapse point for the weight of ICI varies for different path loss exponents.

We compare TCG and CGI to show the collapse in Figure 6. The x-axis is the weight of ICI, so that we could easily see the collapse of the PSNE of the CGI model and the degradation of the system performance with regard to the severity of the ICI. Note that curves for TCG in Figure 6 correspond to the PSNE, while curves for CGI do not correspond to the PSNE, but the average feature of the CGI model. As explained for Figures 4a and 5b, once a device collapses to the macrocell, the PSNE collapses to all zeros without any equilibrium between N_i and zero. Therefore, curves for CGI in Figure 6a, c and e actually show the average of $n_i, i = 1, ..., 5$ for a number of rounds of simulations. Since the devices' deployment and the BSs' locations vary round by round, the collapse points vary, as well. Actually, in each round, the collapse points for different picocells may not be the same either due to the difference of their locations. The average value of n_i for a given cell radius and the weight of ICI can be considered as an average measure of CS preference between picocells and the macrocell. Seen from each subfigure above, the PSNE has larger probability to collapse when the weight of ICI becomes larger, indicating the impact of ICI on the PSNE. Comparing the three subfigures, when the path loss exponent is small, PSNE collapse in a relatively small weight of ICI, indicating the severity of ICI with regard to the path loss exponent.

In Figure 6b, d and f, spatial spectral efficiency with Path Losses 2, 3 and 4 are shown, respectively. The spatial spectral efficiency at each point in each curve is calculated as the summation of all of the devices' total capacity divided by the system bandwidth and the macrocell disc area (in km^2). We can see that the average spatial spectral efficiency decreases after the PSNE collapses. Note that, TCG does not consider the ICI at all, so its PSNE and corresponding average spatial spectral efficiency do not change along with the weight of ICI, as shown in all of the above subfigures.

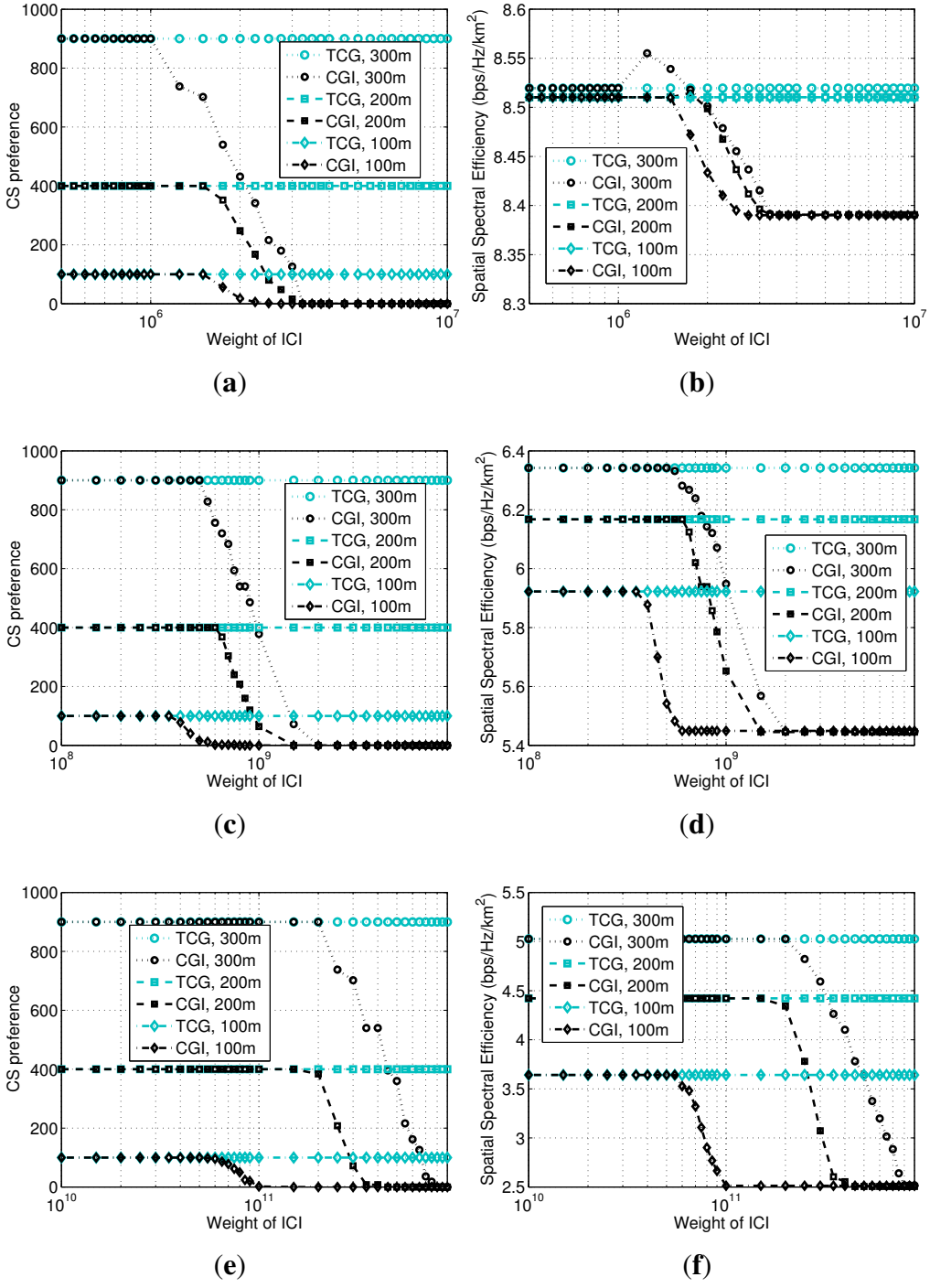

Figure 6. Impact of ICI on CS preference and spatial spectral efficiency using TCG and the congestion game with ICI (CGI). (**a**) Path Loss 2 (free space); (**b**) Path Loss 2 (free space); (**c**) Path Loss 3 (suburbs); (**d**) Path Loss 3 (suburbs); (**e**) Path Loss 4 (downtown); (**f**) Path Loss 4 (downtown).

As we know, for the macrocell, its advantage is the low ICI, while the disadvantage is the small available bandwidth due to the large number of connected devices. By contrast, for the picocells, the advantage is the large available bandwidth, while the disadvantage is severe ICI from the macrocell. Therefore, it is not difficult to understand the simulation results in Figure 6. Devices approaching

picocell BSs obtain larger spectral efficiency by using picocells because of the larger amount of obtained bandwidth and better channel condition to these BSs. When the radii of the picocells are large, more devices will change their preferences during the collapse, so the decrement of spatial spectral efficiency will be large, which is clearly shown in all of the above subfigures. When the path loss exponent becomes larger, the difference of the channel conditions to picocells and the macrocell becomes larger, so the decrement of the spatial spectral efficiency can be very large when the PSNE collapses, which is clear by comparing Figure 6d, f with Figure 6b.

Besides, there is a small augmentation in Figure 6b before the performance collapses, this happens occasionally when the transmission power of picocell devices, the ICI and the picocell radius coincide. In detail, when the picocell radius and the ICI are both large, but the transmission power is relatively small, devices on the edge of a picocell's coverage area should select the macrocell to guarantee system optimality.

5.3. Impact of ICI by Comparing CGC-FFR and CGC-OFD

The configuration for this subsection is similar to Section 5.2, except for the bandwidth and the transmission power are configured as follows. For CGC-FFR, the whole system bandwidth is used in the same way as before. By contrast, for CGC-OFD, the whole bandwidth is divided into two portions, *i.e.*, 2/3 for the macrocell and 1/3 for each picocell. The transmission powers for the picocells with 100 m radii are variable for the x-axis, from -80–20 dBm, while the transmission powers for the picocells with 200 m and 300 m radii are calculated with an augmentation as before to guarantee the increment of the picocell radii, *i.e.*, 6 and 9.5 dBm augmentation for a path loss exponent equaling two; 9 and 14.3 dBm augmentation for a path loss exponent equaling three; and 12 and 19 dBm augmentation for a path loss exponent equaling four. Note that the transmission power of a device selecting a picocell should not be as low as -80 dBm, but we keep the x-axis range large to show the collapse clearly and to compare between CGC-FFR and CGC-OFD.

Figure 7a,c,e shows the collapse of the PSNE for a path loss exponent equaling 2, 3 and 4, respectively. We can see that, when the transmission power of picocells decreases, both of the two games' PSNE collapse. The difference is that CGC-OFD keeps a number of devices selecting picocells in the normal transmission power range, while the ICI in CGC-FFR already makes the PSNE collapse to the macrocell. Besides, by increasing the path loss exponent, the gap between the curves of CGC-FFR and CGC-OFD becomes smaller. That is because the large path loss exponent decreases ICI, hence reducing the difference of the two games. Based on the analysis in Figure 4b and our experience with extensive simulations, the collapse feature of CGC is different from that of CGI. Instead of suddenly collapsing to all zeroes, the PSNE of CGC decreases gradually from N_i to zero, little by little.

The system's average spatial spectral efficiencies with a path loss exponent equaling 2, 3 and 4 are shown in Figure 7b,d,f, respectively. Different from the previous subfigures showing a saturated point where a curve becomes flat, curves in these three subfigures will keep on increasing along with the increase of the transmission power of picocells. We can see that, first, the curves of CGC-FFR are higher than those of CGC-OFD, indicating that, suffering severe ICI, it is still suggested to reuse the frequency. Second, when the path loss exponent is large, the difference of the spatial spectral efficiencies of the

two games decreases due to the decrease of ICI. Third, the curves with larger picocells have better system performance, indicating that, seen from the system's point of view, it is still important to keep a number of devices on the side of picocells, *i.e.*, the PSNE collapsing to the macrocell is generally an undesired result.

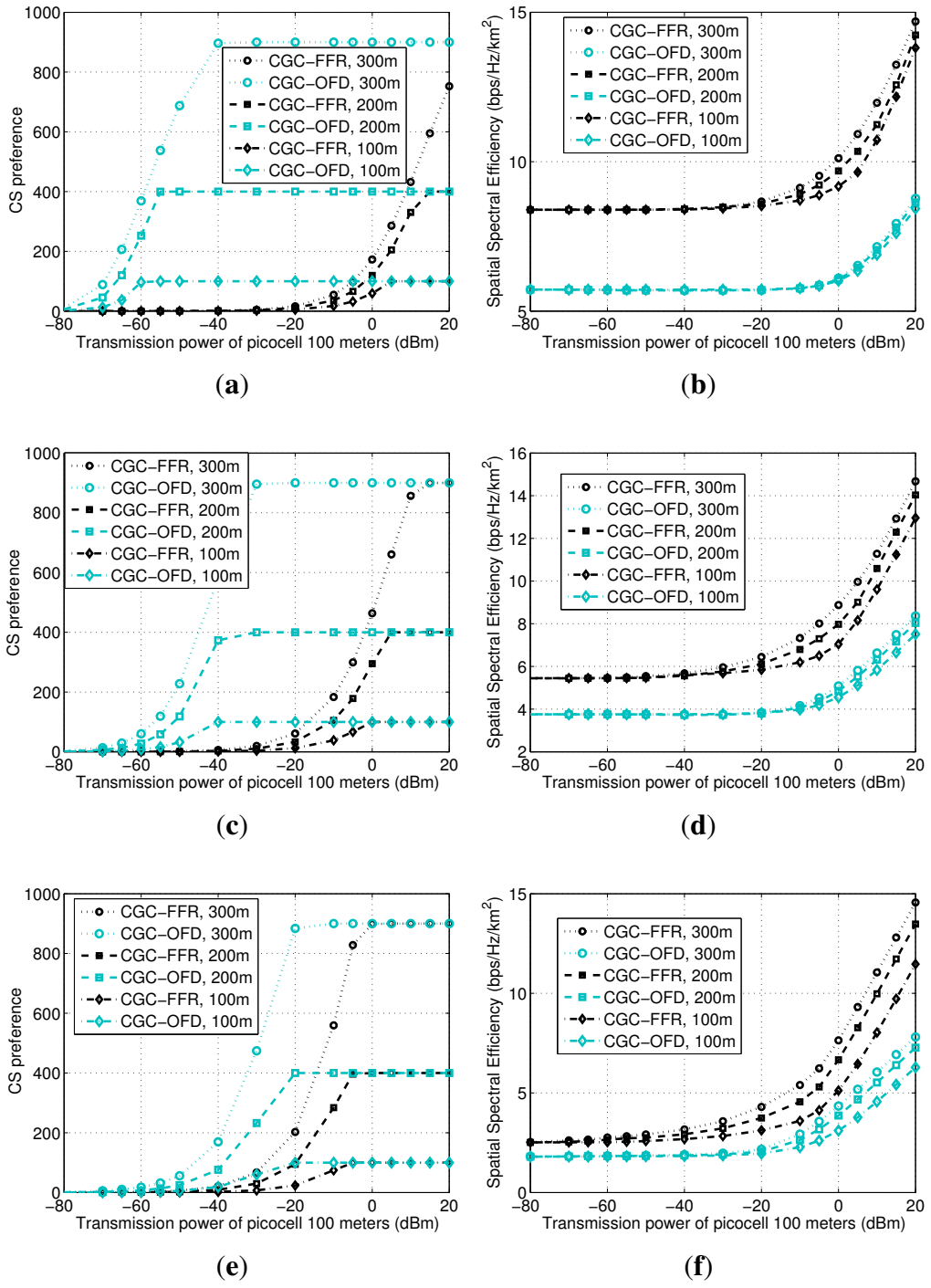

Figure 7. Impact of ICI on CS preference and spatial spectral efficiency using CGC-fractional frequency reuse (FFR) and CGC-orthogonal frequency division (OFD). (**a**) Path Loss 2 (free space); (**b**) Path Loss 2 (free space); (**c**) Path Loss 3 (suburbs); (**d**) Path Loss 3 (suburbs); (**e**) Path Loss 4 (downtown); (**f**) Path Loss 4 (downtown).

6. Conclusions

HCNs and IoT have been considered to form a new wireless network paradigm to evolve the mobile communication system toward 5G, while the CS game among densely-deployed sensor and mobile devices in HCNs became one of the key issues and challenges. For a CS game undergoing severe ICI, the congestion game model was found to be a suitable methodology for this study. In this article, we embedded ICI into the congestion game and theoretically identified the PSNE with three theorems. The closed-form expression for the ICI was calculated and helped validate the three theorems. We conclude that, on the one hand, the CS game among a large amount of densely-deployed devices can be considered from the statistical point of view by integrals, which made this game able to be solved with closed-form expressions. On the other hand, the PSNE of such a game may suddenly collapse to the macrocell under the impact of severe ICI, and the system performance, in terms of average spatial spectral efficiency, could be severely degraded by this collapse phenomenon. Therefore, this study should be quite helpful to design the future CS scheme for dense devices in an integrated environment with HCNs and IoT. Our future work involves the design of a CS scheme fitting for generalized scenarios, such as different traffic types, device types and user preferences, as well as device mobility. Meanwhile, we will theoretically consider a more generalized cell deployment, *i.e.*, the irregular deployment of BSs with Voronoi cell boundaries.

Acknowledgments

This work was supported by the National Natural Science Foundation of China under Grant No. 61501160, also supported by the Fundamental Research Funds for the Central Universities of China under Grant No. 2015HGCH0013.

Author Contributions

Lusheng Wang substantially contributed to problem formulation, system model design, the proposal of all of the theorems and the preparation of most of the sections. Yamei Wang substantially contributed to the simulations and the preparation of the corresponding sections. Zhizhong Ding substantially contributed to the design and guidance of the study, as well as the writing of the Introduction. Xiumin Wang substantially contributed to the proof of the theorems and the writing of the corresponding content.

Conflicts of Interest

The authors declare no conflict of interest.

Appendix

Define:

$$x = \sum_{j \in \mathbf{DV}_{All}} \frac{1}{d_{ij}^2} - \sum_{j \in \mathbf{DV}_i} \frac{1}{d_{ij}^2} \tag{A1}$$

$$y = \sum_{j \in \mathbf{DV}_\alpha} \frac{1}{d_{\alpha j}^2} \tag{A2}$$

Equation (12) can be represented by:

$$I_{0i} = \frac{GP_0}{N_0 - \sum_\alpha n_\alpha}(x - \sum_{\alpha \neq i} y) \tag{A3}$$

To obtain I_{0i}, we should derive x and y, respectively. For x, we establish the polar coordinate system, as shown in Figure A1a. The picocell BS_i is exactly at the pole, while the macrocell BS_0 is at (D_{0i}, π). Thus, the equation of the coverage border circle for BS_0 and the circle formed by $\mathbf{DV}_i$ are:

$$s^2 + D_{0i}^2 + 2sD_{0i}\cos\theta = R_0^2 \tag{A4}$$

$$s = r \tag{A5}$$

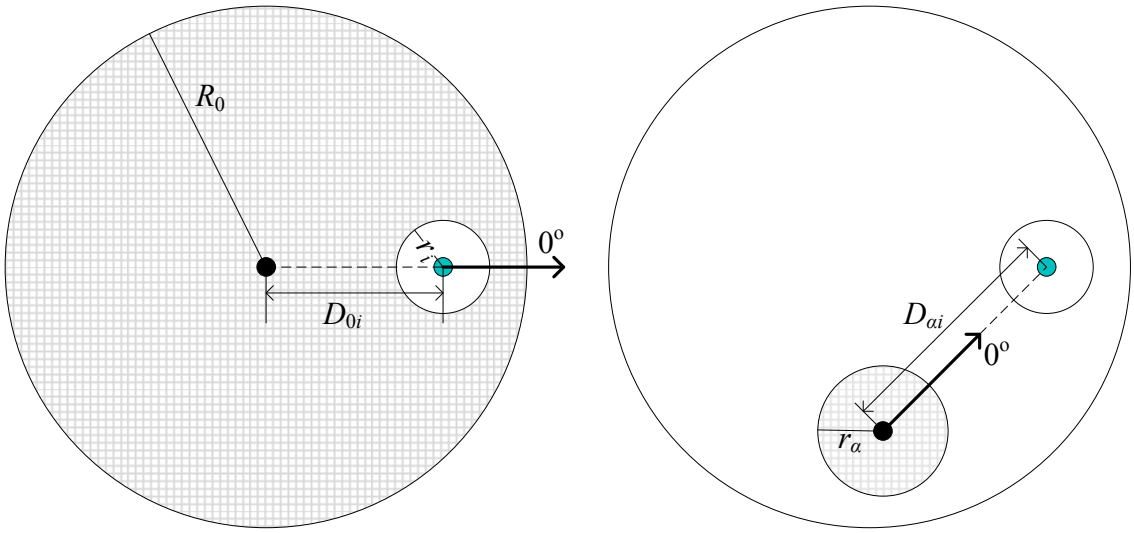

Figure A1. The polar coordinate systems for calculating the ICI. (**a**) To calculate x; (**b**) to calculate y.

Equation (A4) is a quadratic equation of s, which can be solved by the quadratic formula as:

$$s = \sqrt{R_0^2 - D_{0i}^2 \sin^2\theta} - D_{0i}\cos\theta \tag{A6}$$

Equation (A6) provides the relationship between s and θ. Note that the other solution is negative, which cannot be used to represent the distance.

Based on the above analysis, x can be rewritten as:

$$\begin{aligned} x &= \frac{N_0}{\pi R_0^2}\int_0^{2\pi}\int_{r_i}^{\sqrt{R_0^2 - D_{0i}^2\sin^2\theta} - D_{0i}\cos\theta} \frac{1}{s^2} s\,ds\,d\theta \\ &= \frac{2N_0}{\pi R_0^2}\left\{\int_0^{\pi}[\ln(\sqrt{R_0^2 - D_{0i}^2\sin^2\theta} - D_{0i}\cos\theta)]d\theta - \pi\ln r_i\right\} \end{aligned} \tag{A7}$$

To solve the above integral, let:

$$\begin{aligned} z &= \int_0^{\pi} \ln(\sqrt{R_0^2 - D_{0i}^2 \sin^2\theta} - D_{0i}\cos\theta)d\theta \\ &= \int_0^{\pi} \ln\Big[\frac{(\sqrt{R_0^2 - D_{0i}^2 \sin^2\theta} - D_{0i}\cos\theta)}{(\sqrt{R_0^2 - D_{0i}^2 \sin^2\theta} + D_{0i}\cos\theta)} \cdot (\sqrt{R_0^2 - D_{0i}^2 \sin^2\theta} + D_{0i}\cos\theta)\Big]d\theta \\ &= \int_0^{\pi} \ln\Big[\frac{R_0^2 - D_{0i}^2}{\sqrt{R_0^2 - D_{0i}^2 \sin^2\theta} + D_{0i}\cos\theta}\Big]d\theta \\ &= \pi\ln(R_0^2 - D_{0i}^2) - \int_0^{\pi} \ln\big[\sqrt{R_0^2 - D_{0i}^2 \sin^2\theta} + D_{0i}\cos\theta\big]d\theta \end{aligned} \tag{A8}$$

Let $\phi = \pi - \theta$, we find:

$$\begin{aligned} z &= \pi\ln(R_0^2 - D_{0i}^2) - \int_{\pi}^{0} \ln\big[\sqrt{R_0^2 - D_{0i}^2 \sin^2(\pi-\phi)} + D_{0i}\cos(\pi-\phi)\big]d(\pi-\phi) \\ &= \pi\ln(R_0^2 - D_{0i}^2) - \int_0^{\pi} \ln\big[\sqrt{R_0^2 - D_{0i}^2 \sin^2\phi} - D_{0i}\cos\phi\big]d\phi \\ &= \pi\ln(R_0^2 - D_{0i}^2) - z \end{aligned} \tag{A9}$$

We obtain:

$$z = \frac{\pi}{2}\ln(R_0^2 - D_{0i}^2) \tag{A10}$$

Taking Equation (A10) into (A7), we obtain:

$$\begin{aligned} x &= \frac{2N_0}{\pi R_0^2}\big[\frac{\pi}{2}\ln(R_0^2 - D_{0i}^2) - \pi\ln r_i\big] \\ &= \frac{N_0}{R_0^2}\big[\ln(R_0^2 - D_{0i}^2) - \ln\frac{R_0^2}{N_0} - \ln n_i\big] \end{aligned} \tag{A11}$$

To calculate y, we establish the polar coordinate system as shown in Figure A1b, then:

$$y = \frac{N_0}{\pi R_0^2}\int_0^{r_\alpha}\int_0^{2\pi} \frac{s}{s^2 + d_{\alpha j}^2 - 2sd_{\alpha j}\cos\theta}d\theta ds \tag{A12}$$

Let $a = d_{\alpha j}^2 + s^2$ and $b = -2d_{\alpha j}s$, we have $a^2 > b^2$, so the above integral becomes:

$$\begin{aligned} y &= \frac{N_0}{\pi R_0^2}\int_0^{r_\alpha} s\int_0^{2\pi} \frac{1}{a + b\cos\theta}d\theta ds \\ &= \frac{N_0}{\pi R_0^2}\int_0^{r_\alpha} \frac{2s}{\sqrt{a^2 - b^2}}\Big[\arctan\big(\sqrt{\frac{a-b}{a+b}}\cdot\tan\frac{\theta}{2}|_0^{\pi}\big) + \arctan\big(\sqrt{\frac{a-b}{a+b}}\cdot\tan\frac{\theta}{2}|_{\pi}^{2\pi}\big)\Big] \\ &= \frac{N_0}{R_0^2}\int_0^{r_\alpha} \frac{2s}{\sqrt{a^2 - b^2}}ds \end{aligned} \tag{A13}$$

Since we assume that the picocells do not overlap with one another, we have $D_{\alpha i} \geq s$, so:

$$\begin{aligned} y &= \frac{N_0}{R_0^2}\int_0^{r_\alpha} \frac{2s}{d_{\alpha j}^2 - s^2}ds \\ &= \frac{N_0}{R_0^2}[\ln D_{\alpha i}^2 - \ln(D_{\alpha i}^2 - r_\alpha^2)] \end{aligned} \tag{A14}$$

Finally, taking Equations (A11) and (A14) into Equation (A3), I_{0i} is obtained as a function of n_i, written as:

$$I_{0i}(n_i) = \frac{N_0 G P_0}{(N_0 - \sum_\alpha n_\alpha) R_0^2} \Big\{ \big[\ln(R_0^2 - D_{0i}^2) - \ln \frac{R_0^2}{N_0} - \ln n_i \big] - \sum_{\alpha \neq i} \big[\ln D_{\alpha i}^2 - \ln(D_{\alpha i}^2 - \frac{R_0^2 n_i}{N_0}) \big] \Big\} \quad \text{(A15)}$$

References

1. Damnjanovic, A.; Montojo, J.; Wei, Y.; Ji, T.; Luo, T.; Vajapeyam, M.; Yoo, T.; Song, O.; Malladi, D. A survey on 3GPP heterogeneous networks. *IEEE Wirel. Commun.* **2011**, *18*, 10–21.
2. Lopez-Perez, D.; Guvenc, I.; de la Roche, G.; Kountouris, M.; Quek, T.Q.S.; Zhang, J. Enhanced intercell interference coordination challenges in heterogeneous networks. *IEEE Wirel. Commun.* **2011**, *18*, 22–30.
3. Yeh, S.P.; Talwar, S.; Wu, G.; Himayat, N.; Johnsson, K. Capacity and coverage enhancement in heterogeneous networks. *IEEE Wirel. Commun.* **2011**, *18*, 32–38.
4. Guo, W.; Wang, S.; Chu, X.; Zhang, J.; Chen, J.; Song, H. Automated small-cell deployment for heterogeneous cellular networks. *IEEE Commun. Mag.* **2013**, *51*, 46–53.
5. Chandrasekhar, V.; Andrews, J.G.; Gatherer, A. Femtocell networks: A survey. *IEEE Commun. Mag.* **2008**, *46*, 59–67.
6. Lin, P.; Zhang, J.; Chen, Y.; Zhang, Q. Macro-femto heterogeneous network deployment and management: From business models to technical solutions. *IEEE Wirel. Commun.* **2011**, *18*, 64–70.
7. Ghosh, A.; Mangalvedhe, N.; Ratasuk, R.; Mondal, B.; Cudak, M.; Visotsky, E.; Thomas, T.A.; Andrews, J.G.; Xia, P.; Jo, H.S.; *et al*. Heterogeneous cellular networks: From theory to practice. *IEEE Commun. Mag.* **2012**, *50*, 54–64.
8. Andrews, J.G. Seven ways that HetNets are a cellular paradigm shift. *IEEE Commun. Mag.* **2013**, *15*, 136–144.
9. Jin, J.; Gubbi, J.; Marusic, S.; Palaniswami, M. An information framework for creating a smart city through internet of things. *IEEE IoT J.* **2014**, *1*, 112–121.
10. Alam, K.M.; Saini, M.; el Saddik, A. Toward social internet of vehicles: Concept, architecture, and applications. *IEEE Access* **2015**, *3*, 343–357.
11. Patel, M.; Wang, J. Applications, challenges, and prospective in emerging body area networking technologies. *IEEE Wirel. Commun.* **2010**, *17*, 80–88.
12. Akyildiz, I.; Pierobon, M.; Balasubramanism, S.; Koucheryavy, Y. The internet of bio-nano things. *IEEE Commun. Mag.* **2015**, *53*, 32–40.
13. Al-Fuqaha, A.; Guizani, M.; Mohammadi, M.; Aledhari, M.; Ayyash, M. Internet of things: A survey on enabling technologies, protocols, and applications. *IEEE Commun. Surv. Tut.* **2015**, doi:10.1109/COMST.2015.2444095, accepted for publication.
14. I, C.-L.; Han, S.; Chen, Y.; Li, G. Trillions of nodes for 5G!? In Proceedings of the IEEE/CIC International Conference on Communications in China, Shanghai, China, 13–15 October 2014; pp. 246–250.

15. Zhang, J.; Shan, L.; Hu, H.; Yang, Y. Mobile cellular networks and wireless sensor networks: Toward convergence. *IEEE Commun. Mag.* **2012**, *50*, 164–169.
16. Yuan, Y.; Zhu, L. Application scenarios and enabling technologies of 5G. *China Commun.* **2014**, *11*, 69–79.
17. Wang, L.; Kuo, G.S. Mathematical modeling for network selection in heterogeneous wireless networks—A tutorial. *IEEE Commun. Surv. Tut.* **2013**, *15*, 271–292.
18. Trestian, R.; Ormond, O.; Muntean, G.-M. Game theory-based network selection: Solutions and challenges. *IEEE Commun. Surv. Tut.* **2012**, *14*, 1212–1231.
19. Malanchini, I.; Cesana, M.; Gatti, N. Network selection and resource allocation games for wireless access networks. *IEEE Trans. Mob. Comput.* **2013**, *12*, 2427–2440.
20. Ibrahim, M.; Khawam, K.; Tohme, S. Congestion games for distributed radio access selection in broadband networks. In Proceedings of the IEEE Global Telecommunications Conference, Miami, FL, USA, 5–9 December 2010; pp. 1–5.
21. Aryafar, E.; Keshavarz-Haddad, A.; Wang, M.; Chiang, M. RAT selection games in HetNets. In Proceedings of the IEEE INFOCOM, Turin, Italy, 14–19 April 2013; pp. 998–1006.
22. Pederson, K.; Wang, Y.; Strzyz, S.; Frederiksen, F. Enhanced inter-cell interference coordination in co-channel multi-layer LTE-advanced networks. *IEEE Wirel. Commun.* **2013**, *20*, 120–127.
23. Zahir, T.; Arshad, K.; Nakata, A.; Moessner, K. Interference management in femtocells. *IEEE Commun. Surv. Tut.* **2013**, *15*, 293–311.
24. Hanly, S.V. An algorithm for combined cell-site selection and power control to maximize cellular spread spectrum capacity. *IEEE J. Sel. Area Commun.* **1995**, *13*, 1332–1340.
25. Zhang, Y.J.; Letaief, K.B. Mutliuser adaptive subcarrier-and-bit allocation with adaptive cell selection for OFDM systems. *IEEE Trans. Wirel. Commun.* **2004**, *3*, 1566–1575.
26. Sang, A.; Wang, X.; Madihian, M.; Gitlin, R.D. A load-aware handoff and cell-site selection scheme in multi-cell packet data systems. In Proceedings of the IEEE Global Telecommunications Conference, Dallas, TX, USA, 29 November–3 December 2004; pp. 3931–3936.
27. Davaslioglu, K.; Ayanoglu, E. Interference-based cell selection in heterogeneous networks. In Proceedings of the Information Theory and Applications Workshop, San Diego, CA, USA, 10–15 February 2013; pp. 1–6.
28. Oh, J.; Han, Y. Cell selection for range expansion with almost blank subframe in heterogeneous networks. In Proceedings of the IEEE International Symposium on Personal Indoor and Mobile Radio Communications, Sydney, Australia, 9–12 September 2012; pp. 653–657.
29. Wang, J.; Liu, J.; Wang, D.; Pang, J.; Shen, G. Optimized fairness cell selection for 3GPP LTE-A macro-pico HetNets. In Proceedings of the IEEE Vehicular Technology Conference (VTC Fall), San Francisco, CA, USA, 5–8 September 2011; pp. 1–5.
30. Wang, T.; Huang, B.; Wang, Y. Bias-based self-organized cell selections for outdoor open-access picocell networks. In Proceedings of the IEEE Wireless Communications and Networking Conference, Shanghai, China, 7–10 April 2013; pp. 1180–1185.
31. Zhao, X.; Wang, C. An asymmetric cell selection scheme for inter-cell interference coordination in heterogeneous networks. In Proceedings of the IEEE Wireless Communications and Networking Conference, Shanghai, China, 7–10 April 2013; pp. 1226–1230.

32. Bembe, M.; Kim, J.; Olwal, T.; Han, Y. Available bandwidth-aware cell selection for expanded regions of small cells adopting ABS. In Proceedings of the International Conference on Convergence, Jeju Island, South Korea, 14–16 October 2013; pp. 632–636.
33. Corroy, S.; Falconetti, L.; Mathar, R. Cell association in small heterogeneous networks: Downlink sum rate and min rate maximization. In Proceedings of the IEEE Wireless Communications and Networking Conference, Paris, France, 1–4 April 2012; pp. 888–892.
34. Madan, R.; Borran, J.; Sampath, A.; Bhushan, N.; Khandekar, A.; Ji, T. Cell association and interference coordination in heterogeneous LTE-A cellular networks. *IEEE J. Sel. Areas Commun.* **2010**, *28*, 1479–1489.
35. Jo, H.-S.; Sang, Y.J.; Xia, P.; Andrews, J.G. Heterogeneous cellular networks with flexible cell association: A comprehensive downlink SINR analysis. *IEEE Trans. Wirel. Commun.* **2012**, *11*, 3484–3495.
36. Li, Q.; Hu, Q.; Wu, G.; Qian, Y. On the optimal mobile association in heterogeneous wireless relay networks. In Proceedings of the IEEE INFOCOM, Orlando, FL, USA, 25–30 March 2012; pp. 1359–1367.
37. Ye, Q.; Rong, B.; Chen, Y.; Caramanis, C.; Andrews, J.G. Towards an optimal user association in heterogeneous cellular networks. In Proceedings of the IEEE Global Telecommunications Conference, Anaheim, CA, USA, 3–7 December 2012; pp. 4143–4147.
38. Li, Q.; Xu, Y.; Hu, R.Q.; Wu, G. Pricing-based distributed mobile association for heterogeneous networks with cooperative relays. In Proceedings of the IEEE International Conference on Communications, Ottawa, ON, Canada, 10–15 June 2012; pp. 5326–5331.
39. Wei, L.; Xu, Y.; Hu, R.Q.; Qian, Y. An Algebraic framework for mobile association in wireless heterogeneous networks. In Proceedings of the IEEE Global Telecommunications Conference, Atlanta, GA, USA, 9–13 December 2013; pp. 4940–4945.
40. Mesodiakaki, A.; Adelantado, F.; Alonso, L.; Verikoukis, C. Energy-efficiency user association in cognitive heterogeneous networks. *IEEE Commun. Mag.* **2014**, *52*, 22–29.
41. Ye, Q.; Rong, B.; Chen, Y.; Al-Shalash, M.; Caramanis, C.; Andrews, J.G. User association for load balancing in heterogeneous cellular networks. *IEEE Trans. Wirel. Commun.* **2013**, *12*, 2706–2716.
42. Shen, K.; Yu, W. Downlink cell association optimization for heterogeneous networks via dual coordinate descent. In Proceedings of the International Conference on Acoustics, Speech and Signal Processing, Vancouver, BC, Canada, 26–31 May 2013; pp. 4779–4783.
43. Cui, Z.; Adve, R. Joint user association and resource allocation in small cell networks with backhaul constraints. In Proceedings of the Information Sciences and Systems, Prinston, NJ, USA, 19–21 March 2014; pp. 1–6.
44. Qian, L.P.; Zhang, Y.J.; Wu, Y.; Chen, J. Joint base station association and power control via benders' decomposition. *IEEE Trans. Wirel. Commun.* **2013**, *12*, 1651–1665.
45. Kuang, Q.; Speidel, J.; Droste, H. Joint base-station association, channel assignment, beamforming and power control in heterogeneous networks. In Proceedings of the IEEE Vehicular Technology Conference (VTC Spring), Yokohama, Japan, 6–9 May 2012; pp. 1–5.
46. Fooladivanda, D.; Rosenberg, C. Joint resource allocation and user association for heterogeneous wireless cellular networks. *IEEE Trans. Wirel. Commun.* **2013**, *12*, 248–257.

47. Borst, S.; Hanly, S.; Whiting, P. Optimal resource allocation in HetNets. In Proceedings of the IEEE International Conference on Communications, Budapest, Hungary, 9–13 June 2013; pp. 5437–5441.
48. Becvar, Z.; Mach, P. Performance of fast cell selection in two-tier OFDMA networks with small cells. In Proceedings of the IFIP Wireless Days, Dublin, Ireland, 21–23 November 2012; pp. 1–3.
49. Roux, P.; Kamoun, M. Fast cell selection for femtocell based access networks. In Proceedings of the FutureNetw, Warsaw, Poland, 15–17 June 2011; pp. 1–8.
50. Mahmoud, H.A.; Guvenc, I.; Watanabe, F. Performance of open access femtocell networks with different cell-selection methods. In Proceedings of the IEEE Vehicular Technology Conference (VTC Spring), Taipei, Taiwan, 16–19 May 2010; pp. 1–5.
51. Sangiamwong, J.; Saito, Y.; Miki, N.; Abe, T.; Nagata, S.; Okumura, Y. Investigation on cell selection methods associated with inter-cell interference coordination in heterogeneous networks for LTE-advanced downlink. In Proceedings of the European Wireless, Vienna, Austria, 27–29 April 2011; pp. 117–122.
52. Daeinabi, A.; Sandrasegaran, K.; Zhu, X. Performance evaluation of cell selection techniques for picocells in LTE-Advanced networks. In Proceedings of theElectrical Engineering/Electronics, Computer, Telecommunications and Information Technology, Krabi, Thailand, 15–17 May 2013; pp. 1–6.
53. Tarasak, P.; Adachi, K.; Sun, S. Cell selection for TDD two-tier cellular networks based on uplink-downlink capacity. In Proceedings of the IEEE Wireless Communications and Networking Conference, Shanghai, China, 7–10 April 2013; pp. 2016–2021.
54. Domenico, A.; Savin, V.; Ktenas, D. A backhaul-aware cell selection algorithm for heterogeneous cellular networks. In Proceedings of the IEEE International Symposium on Personal Indoor and Mobile Radio Communications, London, UK, 8–11 September 2013; pp. 1688–1693.
55. Thakur, R.; Mishra, S.; Murthy, C.S.R. A load-conscious cell selection scheme for femto-assisted cellular networks. In Proceedings of the IEEE International Symposium on Personal Indoor and Mobile Radio Communications, London, UK, 8–11 September 2013; pp. 2378–2382.
56. Park, J.-S.; Heo, G.-S.; Lee, Y.-H. Capacity maximizing cell-selection in heterogeneous cellular networks. In Proceedings of the SoftCom, Split-Hvar-Dubrovnik, Croatia, 15–17 September 2011; pp. 1–5.
57. Amzallag, D.; Bar-Yehuda, R.; Raz, D.; Scalosub, G. Cell selection in 4G cellular networks. *IEEE Trans. Mob. Comput.* **2013**, *12*, 1443–1455.
58. Domenico, A.; Strinati, E.C.; Duda, A. An energy efficient cell selection scheme for open access femtocell networks. In Proceedings of the IEEE International Symposium on Personal Indoor and Mobile Radio Communications, Sydney, Australia, 9–12 September 2012; pp. 436–441.
59. Lin, J.-S.; Feng, K.-T. Femtocell access strategies in heterogeneous networks using a game theoretical framework. *IEEE Trans. Wirel. Commun.* **2014**, *13*, 1208–1221.
60. Yuan, P.; Liang, Y.-C.; Bi, G. Dynamic access strategy selection in user deployed small cell networks. In Proceedings of the IEEE Wireless Communications and Networking Conference, Shanghai, China, 7–10 April 2013; pp. 3649–3653.

61. Moon, J.-M.; Cho, D.-H. Cell selection algorithm based on competition of users in hierarchical cellular networks. In Proceedings of the IEEE Wireless Communications and Networking Conference, Sydney, Austrilia, 18–21 April 2010; pp. 1–6.
62. Haddad, M.; Wiecek, P.; Altman, E.; Sidi, H. A game theoretic approach for the association problem in two-tier HetNets. In Proceedings of the International Teletraffic Congress, Shanghai, China, 10–12 September 2013; pp. 1–9.
63. Liu, D.; Chen, Y.; Chai, K.K.; Zhang, T. Performance evaluation of Nash bargaining solution based user association in HetNet. In Proceedings of the WiMob, Lyon, France, 7–10 October 2013; pp. 571–577.
64. Gao, L.; Wang, X.; Sun, G.; Xu, Y. A game approach for cell selection and resource allocation in heterogeneous wireless networks. In Proceedings of the IEEE Sensor, Mesh and Ad Hoc Communications and Networks, Salt Lake City, UT, USA, 27–30 June 2011; pp. 530–538.
65. Feng, Z.; Song, L.; Han, Z.; Niyato, D.; Zhao, X. Cell selection in two-tier femtocell networks with open/closed access using evolutionary game. In Proceedings of the IEEE Wireless Communications and Networking Conference, Shanghai, China, 7–10 April 2013; pp. 860–865.
66. Liao, W.; Wang, L.; Li, J. Congestion game with inter-cell interference for cell selection in heterogeneous cellular network. In Proceedings of the IEEE/CIC International Conference on Communications in China, Shanghai, China, 15–17 October 2014; pp. 603–608.
67. Kudo, T.; Ohtsuki, T. Cell selection using distributed Q-learning in heterogeneous networks. In Proceedings of the Asia-Pacific Signal and Information Processing Association Annual Summit and Conference, Kaohsiung, Taiwan, 29 October–1 November 2013; pp. 1–6.
68. Tan, X.; Luan, X.; Cheng, Y.; Liu, A.; Wu, J. Cell selection in two-tier femtocell networks using Q-learning algorithm. In Proceedings of the International Conference on Advanced Communication Technology, PyeongChang, Korea, 16–19 February 2014; pp. 1031–1035.
69. Dhahri, C.; Ohtsuki, T. Q-learning cell selection for femtocell networks: Single- and multi-user case. In Proceedings of the IEEE Global Telecommunications Conference, Anaheim, CA, USA, 3–7 December 2012; pp. 4975–4980.
70. Nash, J. Non-cooperative games. *Ann. Math.* **1951**, *54*, 286–295.
71. Technical Specification ETSI TS 136 101 V12.6.0: LTE; Evolved Universal Terrestrial Radio Access (E-UTRA); User Equipment (UE) radio transmission and reception. Available online: http://www.etsi.org/deliver/etsi_ts/136100_136199/136101/12.06.00_60/ts_136101v120600p.pdf (accessed on 17 September 2015).
72. Milchtaich, I. Congestion games with player-specific payoff functions. *Games Econ. Behav.* **1996**, *13*, 111–124.

© 2015 by the authors; licensee MDPI, Basel, Switzerland. This article is an open access article distributed under the terms and conditions of the Creative Commons Attribution license (http://creativecommons.org/licenses/by/4.0/).